Designing High Entropy Alloys with Dual fcc and bcc Solid-Solution Phases: Structures and Mechanical Properties

ZHAOWU TANG, SHANG ZHANG, RUIPENG CAI, QING ZHOU, and HAIFENG WANG

High entropy alloys (HEAs) with a single fcc phase are usually ductile but not strong, while HEAs with a single bcc phase have high strength but low ductility. Therefore, the combination of fcc and bcc phases was adopted to optimize the mechanical properties. Based on a latest data collection of reported HEAs with a single fcc phase, with dual fcc and bcc phases, and with a single bcc phase, the current work shows that the average valence electron concentration (VEC) and its standard deviation (δVEC) can describe quantitatively phase selection between the fcc and bcc phases in HEAs. Highest (lowest) hardness, highest (lowest) strength, and lowest (highest) ductility were found at the same critical value of VEC* $\approx$ 6.13 (δVEC* $\approx$ 0.207), which corresponds to the HEA with a single bcc (fcc) phase. The current work provides some quantitative rules for designing HEAs with dual fcc and bcc phases as well as modulating strength and ductility.

https://doi.org/10.1007/s11661-019-05131-1

I. INTRODUCTION

ALLOY design in the past was limited to either one principal element (*e.g.*, the Ni-based superalloys) or two (*e.g.*, the TiAl-based superalloys). Their properties were optimized by a minor addition of other elements. In 2004, a new concept of alloy design based on multi-principal elements was introduced independently.[1,2] Cantor *et al.*[1] prepared the alloys with up to 20 elements in equal atom fraction and reported the CoCrFeNiMn alloy with a single fcc solid-solution phase. In contrast to the general understanding of binary and ternary phase diagrams, in which many intermetallic compounds are formed within the center, Yeh *et al.*[2] pointed out that the high mixing entropy of alloys with multiprincipal elements might make the solid-solution phases more stable. A high entropy alloy (HEA) was then defined as an alloy containing at least five principal elements, each of which has a composition range between 5 and 35 at. pct and possesses a high mixing entropy at their liquid state or high-temperature solid-solution state.[3]

Nowadays, HEAs play an important role in alloy design, ascribing to their superb properties such as excellent fracture resistance at cryogenic temperatures,[4] exceptional combination of strength and ductility,[5,6] and outstanding wear resistance.[7] Although the terminology of such alloys is under debate (*e.g.*, HEAs[3] followed by the current work, multiprincipal alloys,[1] or complex concentrated alloys[8]), studies have become focused on the center region of phase diagrams where uncountable possible combinations of four, five, six, or even greater numbers of elements are available[9] to obtain potential alloys with desired properties. In this sense, the classical trial and error method becomes challenging because a large number of experimental trials are needed to find appropriate HEAs.[10] This is the reason why designing HEAs becomes important.[8,11–13]

According to Gao *et al.*,[13] there are three main approaches for designing HEAs, *i.e.*, the empirical parameters,[14–39] the CALPHAD method,[9,40–42] and the first-principle calculations.[43–49] The empirical parameters can provide some simple design rules. Their reliability depends on the parameters themselves and the data collection of reported HEAs. The CALPHAD method is the most effective way for calculating the phase diagrams of HEAs, as long as reliable thermodynamic databases are available. The extrapolation of binary and ternary phase diagrams into high order

ZHAOWU TANG, SHANG ZHANG, RUIPENG CAI, QING ZHOU, and HAIFENG WANG are with the State Key Laboratory of Solidification Processing, Center of Advanced Lubrication and Seal Materials, Northwestern Polytechnical University, Xi'an, 710072 Shaanxi, P.R. China. Contact email: haifengw81@nwpu.edu.cn
Manuscript submitted October 8, 2018.
Article published online February 13, 2019

systems, however, is not reliable. Furthermore, there are no thermodynamic databases for all the reported HEAs. The first-principle calculations are able to predict phase equilibria with the atomic number and the crystal structure as the input parameters. Compared with the CALPHAD method and the first-principle calculations, which require significant computing workload, the empirical parameters provide an easy way for designing HEAs and, thus, were studied intensively.[14–39] Furthermore, their combination with other approaches is able to improve the efficiency of alloy design.[10] For the HEAs with five components in an equal atom fraction, the empirical parameters reduced the trials of 1287 alloys to 127 alloys for designing HEAs with a single fcc or bcc phase. Then, the CALPHAD method reduced the number of potential alloys to 10.

Up to now, a number of empirical parameters have been proposed: δr, standard deviation of dimensionless atomic radius;[14] δd, standard deviation of dimensionless atomic radii in pairs;[27] γ, the ratio of two solid angles of atomic packing for the elements with the largest and smallest atomic sizes[27]; $\varepsilon_{\mathrm{RMS}}$, root-mean-square strain[29]; ΔS_{mix}, the mixing entropy[2]; ΔH_{mix}, the mixing enthalpy[14]; δH_{mix}, standard deviation of dimensionless mixing enthalpy[38]; Ω $(= T_{\mathrm{m}} S_{\mathrm{config}}/|\Delta H_{\mathrm{mix}}|$ with T_{m} the melting temperature and S_{config} the ideal configurational mixing entropy)[15]; μ $(= T_{\mathrm{m}}/T_{\mathrm{SC}}$ with T_{SC} the critical spinodal temperature)[24]; Φ $(= (S_{\mathrm{config}} - S_{\mathrm{H}})/S_{\mathrm{E}}$ with S_{H} the entropy due to the mixing enthalpy and S_{E} the excessive mixing entropy due to the geometrical mismatch)[32]; Λ $(= \frac{S_{\mathrm{config}}}{\delta} r^2)$[30]; S_{corr}, the nonideal configurational mixing entropy[36]; and Θ.[39] Despite their great success,[14–39] most of the empirical parameters aim to design HEAs with a single solid-solution phase.

Actually, HEAs with a single fcc phase are ductile but not strong enough, whereas HEAs with a single bcc phase are very strong but brittle.[50] Lu *et al.*[51–53] designed the eutectic HEAs with dual fcc and bcc phases to obtain an excellent balance between strength and ductility. Similarly, a series of $(\mathrm{FeCoNiCrMn})_{100-x}\mathrm{Al}_x$ (x = 0 to 20 at. pct) HEAs were prepared to show the effects of Al addition on the structure evolution and tensile properties.[54] With the increase of Al addition, the structure changes from a single fcc phase to dual fcc and bcc phases and then to a single bcc phase. The HEAs with a single fcc phase have relatively low strength but high ductility. The HEAs with dual fcc and bcc phases have a sharp increase in strength but decrease in ductility. The HEAs with a single bcc phase are extremely brittle. Moreover, addition of Al into the CoCrCuFeNi HEAs leads to an increase of the volume fraction of bcc phase, thus increasing hardness and wear resistance.[55] Therefore, a combination of fcc and bcc phases is able to optimize the mechanical properties of HEAs, thus highlighting the importance to design HEAs with dual fcc and bcc solid-solution phases.

Guo *et al.*[18] studied the relationship between the average valence electron concentration (VEC) and the structure transition from a single fcc phase to a single bcc phase in HEAs. It was found that the fcc phase is stable for large values of VEC (≥ 8), while the bcc phase is stable for small values of VEC (≤ 6.87). Poletti and Battezzati[24] found that the HEAs with a single fcc (bcc) phase are stable when VEC > 7.5 and $1.6 < e/a < 1.8$ (VEC < 7.5 and $1.8 < e/a < 2.3$). Here, e/a is the average itinerant electron concentration (Section II–C).

Tripathy *et al.*[37] found that the product of S_{E} and the electronegativity difference $\Delta\chi$ (or δr) is also able to describe phase selection between the fcc and bcc phases. Regarding that a large value of VEC is inclined to form an fcc phase and improve ductility while a small value of VEC tends to form a bcc phase and increase strength, VEC was adopted to modulate the strength and ductility of HEAs.[56] The validity of this proposal was proved by adding the Ni (Mo) element with a large (small) value of VEC 10 (6) to the AlCoCrFeNi (CoCrCuFeNi) with a small (large) value of VEC 7.2 (8.8). The study performed by Chen *et al.*,[56] however, did not provide quantitative design rules for HEAs with desired mechanical properties. Tian *et al.*[22] collected the HEAs with a single fcc and a single bcc phase, based on which they found that maximum hardness is achieved when VEC $\approx$ 6.8.

The current work aims to provide quantitative design rules for HEAs from structures (*e.g.*, a single fcc phase, dual fcc and bcc phases, or a single bcc phase) to mechanical properties (*e.g.*, hardness HV, yield strength σ_{y}, and plastic strain ε_{p}). This study is based on the latest data collection of reported HEAs with a single fcc phase, with dual fcc and bcc phases, and with a single bcc phase (Supplementary Tables S-I and S-II). The preparation states of HEAs include as-cast (AC), as-homogenized (AH), as-deformed (AD), and mechanically alloyed (MA). First, the empirical parameters, including those for the atomic size difference δr, δd, γ, and S_{E}, the electronegativity difference $\Delta\chi$ and $\delta\chi$, the electron concentration VEC (or e/a) and its standard deviation δVEC (or $\delta e/a$), and the chemical bond mismatch ΔH_{mix}, δH_{mix}, and $\delta H^0_{\mathrm{mix}}$, and those based on thermodynamic models Ω, Φ, and Θ, are described in Section II. After that, the relationships between the empirical parameters and the structures (the mechanical properties) are studied (Section III). It was found that VEC and δVEC are the parameters that can describe quantitatively phase selection between the fcc and bcc phases in HEAs. δr and S_E relate almost linearly with the mechanical properties. The relationship between VEC (δVEC) and the mechanical properties follows approximately a quadratic (cubic) function. The validity of current design rules is tested by application to some typical HEA systems (Section IV).

II. EMPIRICAL PARAMETERS

The empirical parameters were generally proposed from the Hume–Rothery rules[57] and the thermodynamic model of Takeuchi and Inoue.[58–60] For the former, the stability of a solid-solution phase is controlled by the atomic size difference, the

electronegativity difference, and the electron concentration. For binary alloys, a solid-solution phase is primarily formed when the atomic size difference is less than 15 pct, the electronegativity difference is small, and the electron concentration is within a proper range. For the latter, the difference between the Gibbs free energy of solid and liquid phases is assumed to be proportional to the mixing Gibbs free energy:

$$\Delta G_{\text{mix}} = \Delta H_{\text{mix}} - T\Delta S_{\text{mix}} \quad [1]$$

A solid-solution phase is stable when the mixing entropy is able to restrain the tendencies of ordering and segregation. This means that a solid-solution phase is stable when the chemical bond mismatch is small or its effect can be offset by other factors.

A. *Atomic Size Difference*

The atomic size difference is a key factor for designing HEAs, *e.g.*, a small value indicates a high possibility for the formation of a single solid-solution phase, a large value tends to form the amorphous phase, and otherwise HEAs with multiphases are formed.[14,38] To describe the comprehensive effect of atomic size difference, a standard deviation of dimensionless atomic radius δr was introduced by Zhang *et al.*[14] For an HEA with n components,

$$\delta r = \sqrt{\sum_{i=1}^{n} c_i \left(1 - \frac{r_i}{\bar{r}}\right)^2} \quad [2]$$

where r_i is the atomic radius of component i and $\bar{r} = \sum_{i=1}^{n} c_i r_i$ is the average atomic radius. Similar to δr, the standard deviation of the dimensionless atomic radius in pairs δd was adopted by Wang *et al.*[27]:

$$\delta d = \sqrt{\sum_{i=1}^{n} \sum_{j>i}^{n} c_i c_j \left(1 - \frac{r_i + r_j}{2\bar{r}}\right)^2} \quad [3]$$

Further, the solid angles of atomic packing for the elements with the largest and smallest atomic sizes (ω_{L}, ω_{S}) were introduced. Their ratio γ was chosen to describe the geometrical mismatch and topological instability in atomic packing:

$$\gamma = \frac{\omega_{\text{S}}}{\omega_{\text{L}}} = \frac{\left(1 - \sqrt{\frac{(r_{\text{S}}+\bar{r})^2 - \bar{r}^2}{(r_{\text{S}}+\bar{r})^2}}\right)}{\left(1 - \sqrt{\frac{(r_{\text{L}}+\bar{r})^2 - \bar{r}^2}{(r_{\text{L}}+\bar{r})^2}}\right)} \quad [4]$$

where r_{L} and r_{S} are the radius of the largest and smallest atoms. Thermodynamically, the atomic size difference can be described by the geometrical mismatch entropy S_{E}.

According to Mansoori *et al.*,[61]

$$\frac{S_{\text{E}}}{k_{\text{B}}} = \frac{F - F^{\text{id}}}{k_{\text{B}}T} - \ln Z - (3 - 2\xi)(1 - \xi)^{-2} + 3 + \ln\left[\left(1 + \xi + \xi^2 - \xi^3\right)(1 - \xi)^{-3}\right] \quad [5]$$

where

$$\frac{F - F^{\text{id}}}{k_{\text{B}}T} = -\frac{3}{2}(1 - y_1 + y_2 + y_3) + (3y_2 + 2y_3)(1 - \xi)^{-1} + \frac{3}{2}\left(1 - y_1 + y_2 - \frac{1}{3}y_3\right)(1 - \xi)^{-2} + (y_3 - 1)\ln(1 - \xi) \quad [6]$$

$$Z = \left[\left(1 + \xi + \xi^2\right) - 3\xi(y_1 + y_2\xi) - \xi^3 y_3\right](1 - \xi)^{-3} \quad [7]$$

$$y_1 = \sum_{i=1}^{n} \sum_{j>i}^{n} \Delta_{ij}\left(d_i + d_j\right)\left(d_i d_j\right)^{-1/2} \quad [8]$$

$$y_2 = \sum_{i=1}^{n} \sum_{j>i}^{n} \Delta_{ij} \sum_{k=1}^{n} \frac{\xi_k}{\xi} \frac{\left(d_i d_j\right)^{-1/2}}{d_k} \quad [9]$$

$$y_3 = \left[\sum_{i=1}^{n} \left(\frac{\xi_i}{\xi}\right)^{2/3} c_i^{1/3}\right]^3 \quad [10]$$

$$\Delta_{ij} = \frac{\left(\xi_i \xi_j\right)^{1/2}}{\xi} \frac{\left(d_i + d_j\right)^2}{d_i d_j} \left(c_i c_j\right)^{1/2} \quad [11]$$

$$\xi = \sum_{i=1}^{n} \xi_i = \sum_{i=1}^{n} \frac{1}{6}\pi\rho c_i d_i^3 \quad [12]$$

Here, d_i is the atomic diameter of component i, ρ is the number density, ξ is the overall atomic packing fraction for a given ρ, and k_{B} is the Boltzmann constant.

B. *Electronegativity Difference*

Electronegativity χ is a chemical property that describes the tendency of an atom to attract a shared pair of electrons toward itself. The electronegativity difference can be described by the standard deviation of electronegativity[17]:

$$\Delta\chi = \sqrt{\sum_{i=1}^{n} c_i (\chi_i - \bar{\chi})^2} \quad [13]$$

where χ_i is the Pauling electronegativity of component i and $\bar{\chi} = \sum_{i=1}^{n} c_i \chi_i$ is the average electronegativity. Similarly, the electronegativity difference can be described by standard deviation of dimensionless electronegativity; *i.e.*,

$$\delta\chi = \sqrt{\sum_{i=1}^{n} c_i \left(1 - \frac{\chi_i}{\bar{\chi}}\right)^2} \quad [14]$$

The electronegativity difference was found to be able to describe phase selection between the fcc and bcc phases,[24] but it was not given much attention.[17,37]

C. *Electron Concentration and Its Standard Deviation*

The electron concentration can be defined by either the average number of itinerant electrons per atom, e/a, or the number of total electrons including the d-electrons accommodated in the valence band, VEC. For the former, we have

$$e/a = \sum_{i=1}^{n} c_i (e/a)_i \quad [15]$$

For the latter, we have

$$\mathrm{VEC} = \sum_{i=1}^{n} c_i (\mathrm{VEC})_i \quad [16]$$

Here, $(e/a)_i$ and $(\mathrm{VEC})_i$ are the itinerant and the VEC of component i. (A detailed description of e/a and VEC is available in References 17, 18, and 24 and the references therein.) In the present work, the standard deviation of dimensionless electron concentration is introduced:

$$\delta e/a = \sqrt{\sum_{i=1}^{n} c_i \left(1 - \frac{(e/a)_i}{e/a}\right)^2} \quad [17]$$

$$\delta\mathrm{VEC} = \sqrt{\sum_{i=1}^{n} c_i \left(1 - \frac{(\mathrm{VEC})_i}{\mathrm{VEC}}\right)^2} \quad [18]$$

In this way, both the average electron concentration and the electron concentration difference are considered to design HEAs.

D. *Chemical Bond Mismatch*

For an HEA with n elements, the mixing enthalpy ΔH_{mix} is given by[58]

$$\Delta H_{\mathrm{mix}} = \sum_{i=1}^{n} \sum_{j>i}^{n} \Omega_{ij} c_i c_j = \sum_{i=1}^{n} \sum_{j>i}^{n} 4 H_{\mathrm{mix}}^{ij} c_i c_j \quad [19]$$

where H_{mix}^{ij} is the mixing enthalpy between components i and j. The mixing enthalpy actually describes the tendencies of ordering and segregation; *e.g.*, a negative ΔH_{mix} makes different components combine to form intermetallic compounds, while a positive ΔH_{mix} makes a mix of different components difficult and leads to segregation in solids.[15] In this sense, a small value of $|\Delta H_{\mathrm{mix}}|$ results in the formation of HEAs with solid-solution phases. However, this is not always the case because a negligible $|\Delta H_{\mathrm{mix}}|$ does not guarantee that the mixing enthalpy of each atomic pair is negligibly small.[38] Furthermore, it was found that both the chemical bond mismatch between different atomic pairs and the geometrical mismatch between different components induce energy fluctuations in an alloy and make the mixing entropy change from an ideal to a nonideal one.[36] Similar to the standard deviation of the dimensionless atomic radius δr that characterizes the atomic size difference, the standard deviation of dimensionless mixing enthalpy was introduced to describe the chemical bond mismatch[38]:

$$\delta H_{\mathrm{mix}} = \frac{\sqrt{\sum_{i=1}^{n} \sum_{j>i}^{n} c_i c_j \left(H_{\mathrm{mix}}^{ij} - \Delta H_{\mathrm{mix}}\right)^2}}{\mathrm{k_B} T_m} \quad [20]$$

The relationship between the normalized energy fluctuation by He *et al.*,[36] x_c, at the melting temperature and the standard deviation of dimensionless mixing enthalpy is $x_c | T = T_m = 2\sqrt{\delta H_{\mathrm{mix}}}$. Because it is the difference between H_{mix}^{ij} and 0 but not between H_{mix}^{ij} and ΔH_{mix} that characterizes the tendencies of ordering and segregation, the standard deviation of dimensionless mixing enthalpy was redefined as[38]

$$\delta H_{\mathrm{mix}}^{0} = \frac{\sqrt{\sum_{i=1}^{n} \sum_{j>i}^{n} c_i c_j \left(H_{\mathrm{mix}}^{ij} - 0\right)^2}}{\mathrm{k_B} T_m} \quad [21]$$

Both δH_{mix} and $\delta H_{\mathrm{mix}}^{0}$ (or $2\sqrt{\delta H_{\mathrm{mix}}}$ and $2\sqrt{\delta H_{\mathrm{mix}}^{0}}$) were found to be able to separate reasonably HEAs with a single solid-solution phase, with multiphases and with an amorphous phase; the latter predicts a little bit better than the former.[38]

E. *Parameters Based on Thermodynamic Models*

In the thermodynamic model of Takeuchi and Inoue[58–60] (Eq. [1]), $|\Delta H_{\mathrm{mix}}|$ is the driving force for ordering or segregation whereas ΔS_{mix} is the resistant force. In the case that ΔS_{mix} is given by S_{config}, the competition between $\mathrm{TS}_{\mathrm{config}}$ and $|\Delta H_{\mathrm{mix}}|$ determines the formation of solid-solution phases; *i.e.*, a larger value of Ω corresponds to a higher possibility for the formation of HEAs with solid-solution phases.[15] It should be mentioned that at the liquid state, the configurational entropy dominated over the enthalpy. If ΔS_{mix} is given by $S_{\mathrm{config}} + S_{\mathrm{E}}$,[58] Eq. [1] can be rewritten as $\Delta G_{\mathrm{mix}} = \Delta H_{\mathrm{mix}} - T\left(S_{\mathrm{config}} + S_{\mathrm{E}}\right)$. When ΔG_{mix} is dominated by ΔS_{mix}, we have $\frac{|\Delta H_{\mathrm{mix}}|}{T\Delta S_{\mathrm{mix}}} << 1$ and $|S_{\mathrm{E}}|/S_{\mathrm{config}} + S_{\mathrm{H}}/S_{\mathrm{config}} << 1$, indicating that both the atom size difference and the mixing enthalpy should be near zero for the formation of HEAs with single solid-solution phases. This is equivalent to the Φ parameter, for which a large value indicates a high

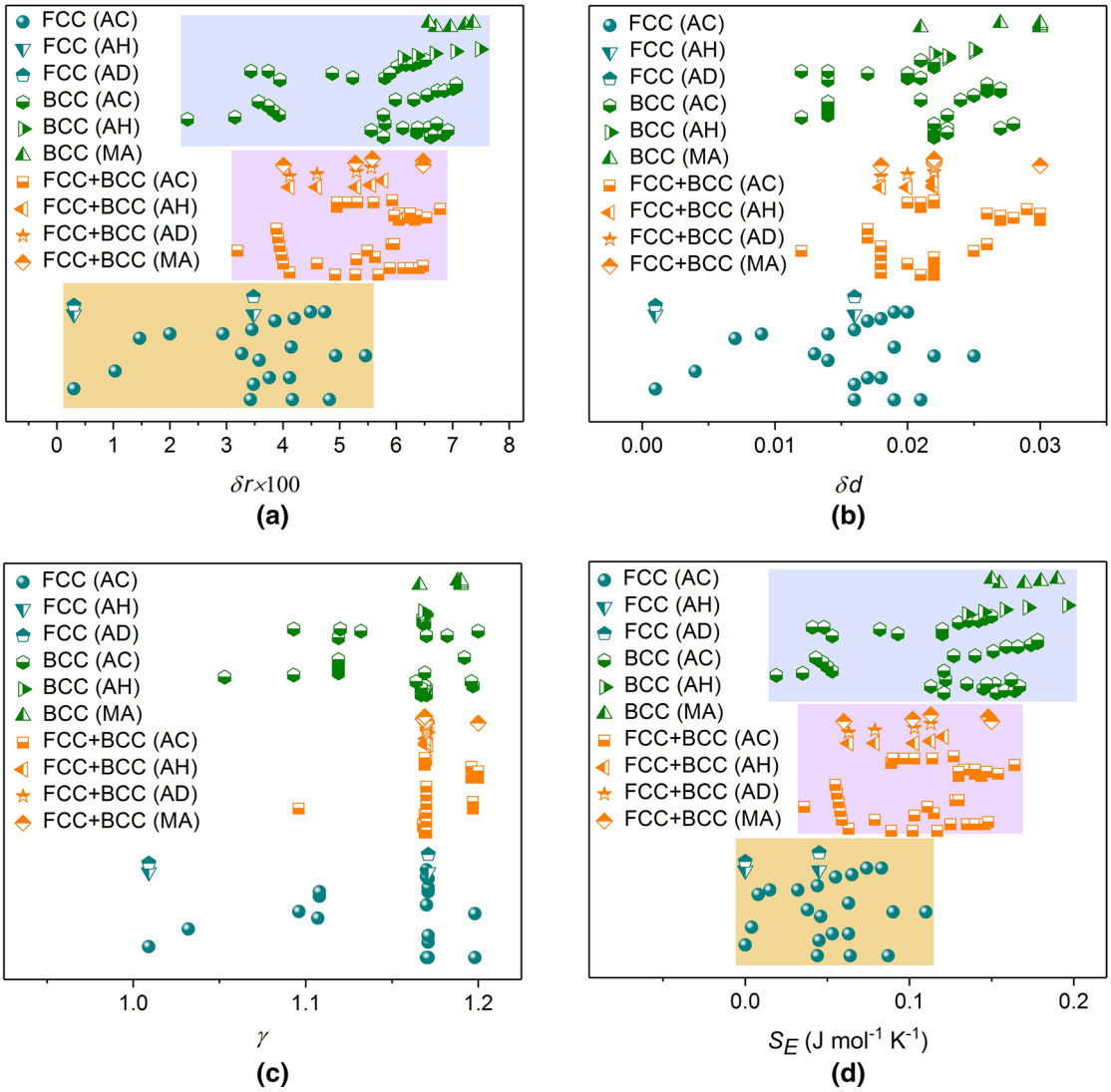

Fig. 1—Effect of atomic size difference on phase selection between the fcc and the bcc phase in HEAs: (*a*) $\delta r \times 100$, (*b*) δd, (*c*) γ, and (*d*) S_{E}.

possibility for the formation of HEAs with a single solid-solution phase.[32]

Noting that the parameters Ω and Φ are based on the average properties of constituent elements, significant deviation of individual properties might make them inapplicable; a Θ parameter that includes not only the average properties (*e.g.*, S_{config}, ΔH_{mix}, and S_{E}) but also the individual properties (*e.g.*, the highest negative (positive) mixing enthalpy $\Delta H_{\mathrm{mix}}^{ij,\mathrm{min}}$ ($\Delta H_{\mathrm{mix}}^{ij,\mathrm{max}}$)) was proposed[39]:

$$\Theta = \frac{|\Delta H_{\mathrm{mix}}|}{T_{\mathrm{m}} S_{\mathrm{config}}} + \frac{\left|\Delta H_{\mathrm{mix}}^{ij,\mathrm{min}}\right|}{T_{\mathrm{m}} S_{\mathrm{config}}} \frac{\left|\Delta H_{\mathrm{mix}}^{ij,\mathrm{max}}\right|}{T_{\mathrm{m}} S_{\mathrm{config}}} \frac{|S_{\mathrm{E}}|}{S_{\mathrm{config}}} \qquad [22]$$

The first, second, and third terms on the right-hand side of Eq. [22] characterize the tendencies for the formation of intermetallic compounds and segregation in solids, while the fourth term stands for the atomic size difference. In other words, both the chemical and geometrical mismatches are integrated into the Θ parameter. For each of four terms, a small value corresponds to a high possibility for the formation of HEAs with a single solid-solution phase.

III. DESIGN RULES

In this section, the relationship between the empirical parameters and the structures (the mechanical properties) is studied based on the current data collection of reported HEAs.

A. *Predicting the Structures*

Figure 1 shows the one-dimensional (1-D) maps for δr, δd, γ, and S_{E}. From Figure 1(a), HEAs with a single fcc phase, with dual fcc and bcc phases, and with a single bcc phase are found when 0.1 pct $< \delta r <$ 5.6 pct, 3.1 pct $< \delta r <$ 6.9 pct, and 2.2 pct $< \delta r <$ 7.6 pct, respectively, even though the evolution tendency could be that a

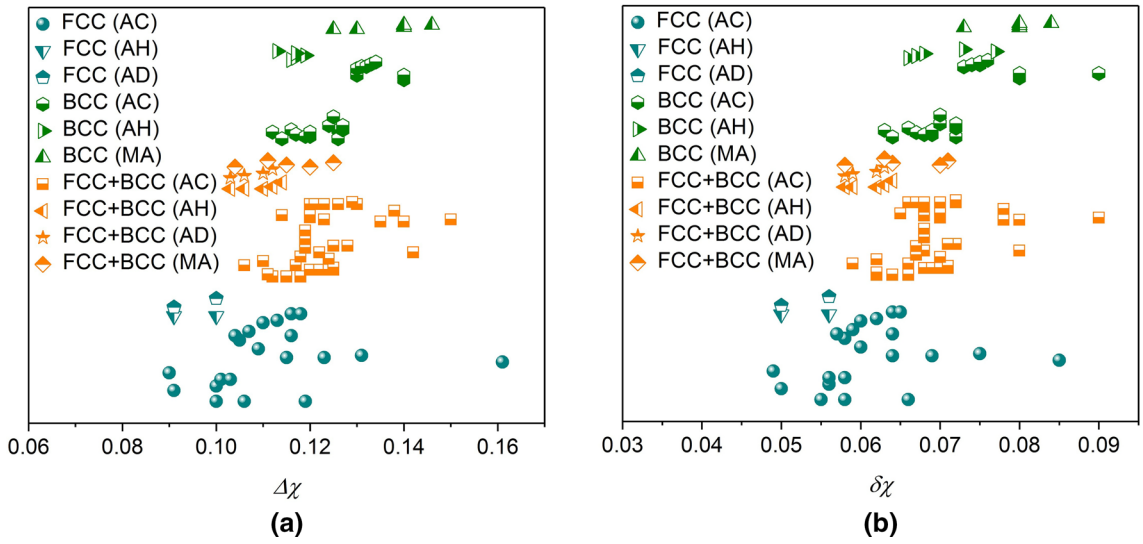

Fig. 2—Effect of electronegativity difference on phase selection between the fcc and bcc phases in HEAs: (*a*) $\Delta\chi$ and (*b*) $\delta\chi$.

small (large) value of δr corresponds to a high possibility for the formation of HEAs with a single fcc (bcc) phase. The region of HEAs with dual fcc and bcc phases is totally within the region of HEAs with a single bcc phase. Different from Tripathy *et al.*,[37] the current work with more data collection of reported HEAs demonstrates that the standard deviation of dimensionless atomic radius is not able to separate reasonably the three regions. For δd, γ, and S_{E}, the same evolution tendency can be found, *i.e.*, a relatively small (large) atomic size difference corresponds to a high possibility for the formation of HEAs with a single fcc (bcc) phase. Because $S_{\mathrm{E}} \sim (\delta r)^2$ holds,[31] the prediction of S_{E} is similar to δr; *e.g.*, HEAs with a single fcc phase, with dual fcc and bcc phases, and with a single bcc phase are found when $0 < S_{\mathrm{E}} < 0.11$ (J mol^{-1} K^{-1}), $0.03 < S_{\mathrm{E}} < 0.17$, and $0.01 < S_{\mathrm{E}} < 0.20$, respectively.

Figure 2 shows the 1-D maps for the electronegativity difference $\Delta\chi$ and $\delta\chi$. It is obvious that for both $\Delta\chi$ and $\delta\chi$, regions of HEAs with dual fcc and bcc phases and with a single bcc phase are within the region of HEAs with a single fcc phase. Even though $\delta\chi$ is able to separate the regions of HEAs with a single solid-solution phase, with a dual solid-solution phase and intermetallic compound,[24] it is insensitive to the crystal structure of solid-solution phase and, thus, is not able to describe phase selection between the fcc and bcc phases, consistent with Tripathy *et al.*[37]

Figure 3 show the 1-D maps for VEC, δVEC, e/a, and $\delta e/a$. One can see that VEC (δVEC) is able to separate the three regions; *i.e.*, HEAs with a single fcc phase, with dual fcc and bcc phases, and with a single bcc phase are found when $7.7 < \mathrm{VEC} < 8.9$ ($0.17 < \delta\mathrm{VEC} < 0.32$), $6.8 < \mathrm{VEC} < 8.5$ ($0.21 < \delta\mathrm{VEC} < 0.46$), and $4.2 < \mathrm{VEC} < 8.2$ ($0.07 < \delta\mathrm{VEC} < 0.22$ or $0.31 < \delta\mathrm{VEC} < 0.54$), respectively. These results are comparable with Guo *et al.*,[18] according to which an fcc (bcc) phase is stable for large (small) values of VEC. For e/a, the region of HEAs with dual fcc and bcc phases is within the region of HEAs with a single bcc phase. For $\delta e/a$, the region of HEAs with a single fcc phase is within the region of HEAs with a single bcc phase. Therefore, phase selection between the fcc and bcc phases is insensitive to the itinerant electron concentration as well as its standard deviation.

Figure 4 shows the effects of mixing enthalpy and chemical bond mismatch on phase selection between the fcc and bcc phases in HEAs. For the former, the region of HEAs with a single bcc (fcc) phase locates at small (large) values and the region of HEAs with dual fcc and bcc phases is totally within the region of HEAs with a single bcc region (Figure 4(a)). Similar results are found for $2\sqrt{\delta H_{\mathrm{mix}}}$ and $2\sqrt{\delta H^0_{\mathrm{mix}}}$, as shown in Figures 4(b) and (c). In contrast to the fact that the chemical bond mismatch plays an important role in the design of HEAs with a single solid-solution phase,[36,38,39] it seems to be irrelevant to the design of HEAs with dual fcc and bcc phases.

Figure 5 shows the predictions of Ω, Φ, and Θ. Such empirical parameters derived from the thermodynamic models include either the chemical effect of mixing enthalpy (*i.e.*, Ω) or the effects of both chemical band mismatch and atomic size difference (*i.e.*, Φ and Θ). Similar to the results represented in Figures 1 and 4, the region of HEAs with dual bcc and fcc phases is totally within the region of HEAs with a single bcc phase; thus, all of these empirical parameters fail to predict phase selection between the fcc and bcc phases in HEAs.

From Figures 1 through 5, phase selection is insensitive to the atomic size difference, the electronegativity difference, the average itinerant electron concentration and its standard deviation, the chemical bond mismatch, as well as a combination of these effects. This is also the case for the empirical parameter $S_{\mathrm{E}}\Delta\chi$ ($S_{\mathrm{E}}\delta r$) adopted by Tripathy *et al.*[42] (not shown here), which is a combination of the atomic size difference and the

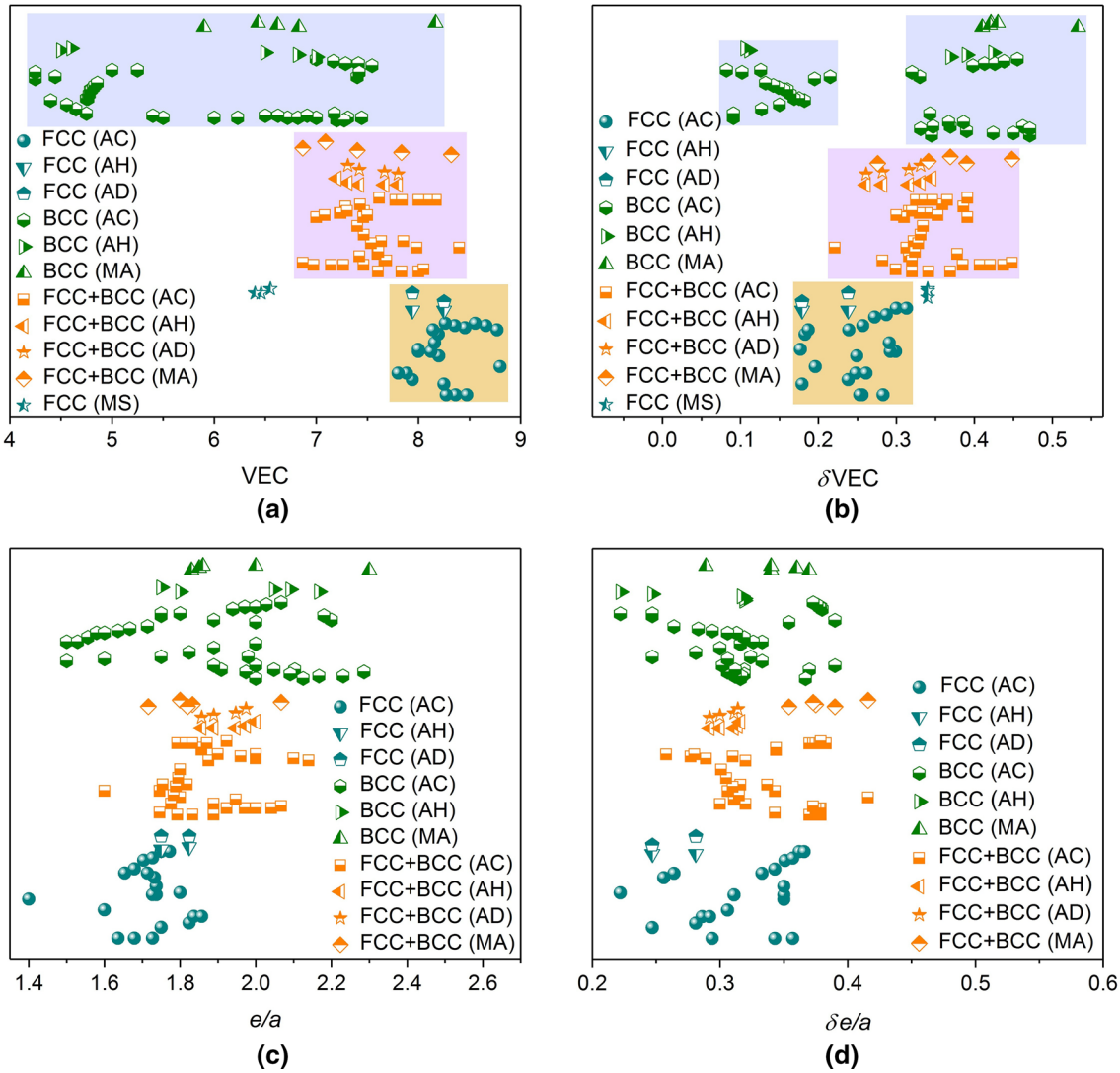

Fig. 3—Effects of electron concentration and electron concentration difference on phase selection between the fcc and bcc phases in HEAs: (*a*) VEC, (*b*) δVEC, (*c*) $\frac{e}{a}$, and (*d*) $\delta\frac{e}{a}$.

electronegativity difference (different empirical parameters for the atomic size difference). The average VEC and its standard deviation are the only parameters that are sensitive to the crystal structure of solid-solution phase. According to Chen *et al.*,[56] a larger (smaller) value of VEC induces higher (lower) atomic bonding forces, so that the alloy tends to form an fcc (bcc) structure with a larger (smaller) atomic packing density. Therefore, δVEC might characterize the difference (fluctuation) in the atomic bonding forces. Accordingly, either a smaller or a larger difference (or value of fluctuation) in the atomic bonding forces tends to form a single bcc phase in HEAs, while an intermediate value indicates the formation of HEAs with a single fcc phase. In the current work, the sufficient condition for designing HEAs with a single fcc phase is VEC $>$ 8.5. For the HEAs with dual bcc and fcc phases (a single bcc phase), it is δVEC $>$ 0.32 (δVEC $<$ 0.17 or δVEC $>$ 0.46). Such rules for designing HEAs with dual bcc and fcc phases are so rigorous that they may lose most of the potential HEAs. Therefore, it is more sensible to design first an HEA with a single fcc (bcc) phase by the necessary condition VEC $>$ 7.7 or 0.17 $<$ δVEC $<$ 0.32 (VEC $<$ 8.2, δVEC $<$ 0.22, or δVEC $>$ 0.31) and then add other elements with lower (higher) values of VEC.[5]

It should be pointed out that Zhang *et al.*[62] studied the effect of nitrogen addition on the structure and mechanical properties of $(Al_{0.5}CrFeNiTi_{0.25})N_x$ high-entropy films by magnetron sputtering (MS). The film is amorphous when $x = 0$ and is transformed to a single fcc phase with increasing addition of nitrogen. The $Al_{0.5}CrFeNiTi_{0.25}$ HEA prepared by casting is a single bcc phase. If these results are included, *e.g.*, as stars in Figures 3(a) and (b), one can see that they are out of the region with a single fcc phase. Indeed, films prepared by MS are quite different from bulk alloys prepared by AC, AH, AD, and MA. Predicting their phase constitution is outside the scope of the current work.

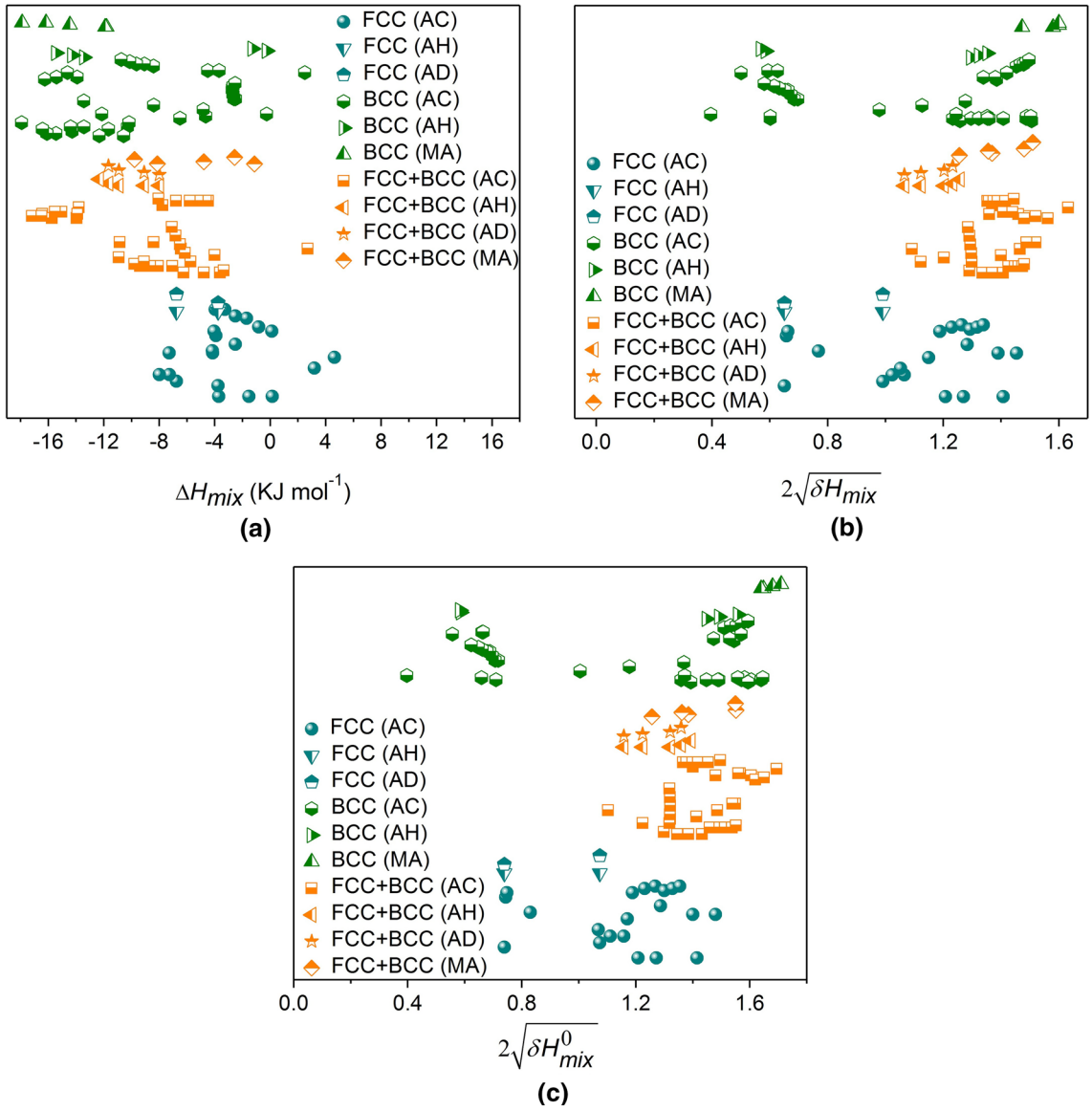

Fig. 4—Effects of mixing enthalpy and the chemical bond mismatch on phase selection between the fcc and bcc phases in HEAs: (*a*) ΔH_{mix}, (*b*) $2\sqrt{\delta \text{H}_{\text{mix}}}$, and (*c*) $2\sqrt{\delta H^{0}_{\text{mix}}}$.

B. *Predicting the Mechanical Properties*

In the work of Tian *et al.*,[22] which aimed to design HEAs with high hardness, VEC and δr were adopted. The former determines the structures and affects the mechanical properties. The latter characterizes the atomic size difference. It is highly related to the atomic stress state in solids and, hence, the mechanical properties. In the current work, the geometrical mismatch entropy, S_{E}, that is frequently used and the standard deviation of VEC, δVEC, that is introduced currently are adopted further to predict the mechanical properties of HEAs.

Figure 6 shows the effects of the atomic size difference, the average VEC, and its standard deviation on hardness HV. Despite its large scatter, hardness HV increases continuously with δr and S_{E} (Figures 6(a) and (b)). If a linear function is adopted, the relationship between HV and δr (S_{E}) is $\text{HV} = 97.1 + 65.2\delta r \times 100$ ($\text{HV} = 206.0 + 2191.3S_{\text{E}}$). With the increase of VEC, HV increases first and then decreases, as shown in Figure 6(c). The relationship between HV and VEC can be well predicted by the quadratic function $\text{HV} = -2177.4 + 888.56\text{VEC} - 71.6\text{VEC}^2$, according to which a critical value of VEC = 6.2 is found at which hardness is a maximum. With the increase of δVEC, HV decreases first and then increases (Figure 6(d)). If a cubic function is adopted to fit the relationship, $\text{HV} = 986.3 - 8592.6\delta\text{VEC} + 29470.8\delta\text{VEC}^2 - 26771.1\text{VEC}^3$

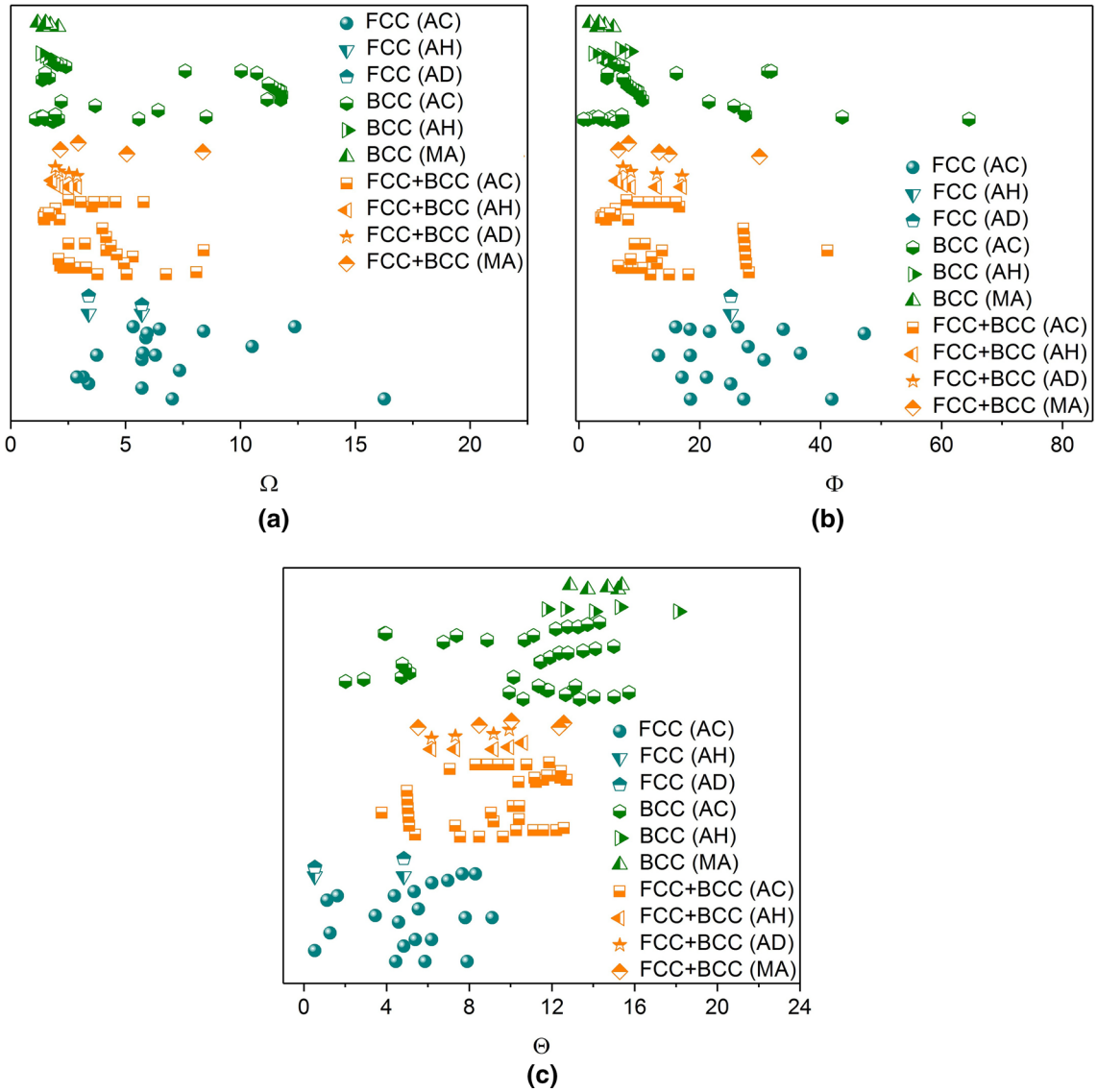

Fig. 5—Effects of (*a*) Ω, (*b*) Φ, and (*c*) Θ on phase selection between the fcc and bcc phases in HEAs.

results according to which a critical value of δVEC = 0.2 is predicted at which hardness is a minimum.

Figure 7 shows the yield strength σ_y as a function of $\delta r \times 100$, S_E, VEC, and δVEC. The relationship between σ_y and $\delta r \times 100$ (S_E, VEC, and δVEC) is completely consistent with that between HV and $\delta r \times 100$ (S_E, VEC, and δVEC). σ_y increases almost linearly with the atomic size difference and the relationships are $\sigma_y = 199.2 + 194.3\delta r \times 100$ and $\sigma_y = 571.7 + 5924.1 S_E$. σ_y increases first with VEC and then decreases, whereas it decreases first with δVEC and then increases. The relationships fitted by the quadratic and the cubic function are $\sigma_y = -7486.7 + 3075.0\text{VEC} - 255.2\text{VEC}^2$ and $\sigma_y = 1665.5 - 3724.2\delta\text{VEC} - 8782.4\delta\text{VEC}^2 + 46957.2\delta\text{VEC}^3$, respectively. The maximum and minimum σ_y are found at VEC = 6.1 and δVEC = 0.23, respectively.

Figure 8 summarizes the effects of the atomic size difference, the average VEC, and its standard deviation on the plastic strain. It is quite obvious that the relationships between the empirical parameters and the plastic strain are completely opposite to those between the empirical parameters and hardness as well as the yield strength. With the increase of atomic size difference, the plastic strain ε_p decreases almost linearly and the relationships are $\varepsilon_P = 46.6 - 4.6\delta r \times 100$ and $\varepsilon_P = 35.6 - 119.4 S_E$ (Figures 8(a) and (b)). ε_p decreases (increases) first with VEC (δVEC) and then increases (decreases) (Figures 8(c)

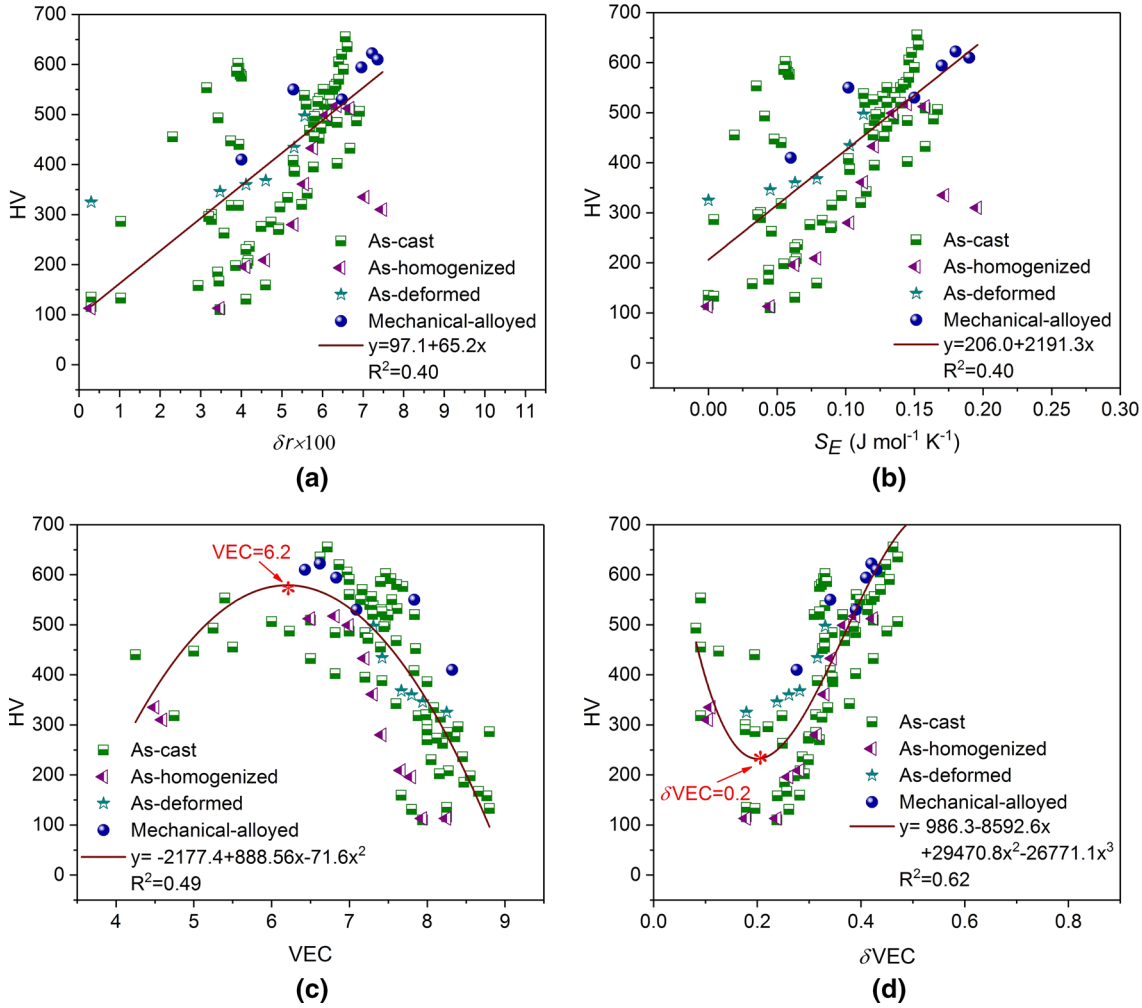

Fig. 6—Hardness HV as a function of (*a*) $\delta r \times 100$, (*b*) S_E, (*c*) VEC, and (*d*) δVEC for HEAs with a single fcc phase, with dual fcc and bcc phases, and with a single bcc phase.

and (d)). $\sigma_y = 224.8 - 72.2\text{VEC} + 6\text{VEC}^2$ ($\sigma_y = -101.6 + 1750.7\delta\text{VEC} - 6974.2\delta\text{VEC}^2 + 8334.5\delta\text{VEC}^3$) holds. Accordingly, the minimum and maximum plastic strains are achieved at VEC = 6.1 and δVEC = 0.19, respectively.

From Figures 6(c) through 8(c), maximum hardness, maximum strength, and lowest ductility are obtained at almost the same value of average VEC, which is $\text{VEC}^* \approx 6.13$ if the three critical values are averaged. It is not far away from VEC = 6.8 at which hardness is maximum in the work of Tian *et al.*[22] According to Figure 3(a), the structure of HEAs at VEC ≈ 6.13 is a single bcc phase, indicating that the strongest but brittle HEA should be the HEA with a single bcc phase and with VEC ≈ 6.13, away from which a sharp decrease (increase) of strength (ductility) is identified. From Figures 6(d) through 8(d), lowest hardness, lowest strength, and maximum ductility are also obtained at similar values of standard deviation of the average VEC, which is $\delta\text{VEC}^* \approx 0.207$, if the three critical values are averaged. According to Figure 3(b), the structure of HEAs at δVEC ≈ 0.207 consists of a single fcc phase. This means that the most ductile but weak HEAs should be the HEA with a single fcc phase and with δVEC ≈ 0.207, away from which a sharp increase (decrease) of strength (ductility) is revealed. Therefore, a modulation between strength and ductility should be achieved by the HEAs with dual fcc and bcc phases, and VEC (δVEC) can vary away from 6.13 (0.207) to obtain a large ductility (a high strength).

IV. APPLICATION TO TYPICAL HEA SYSTEMS

In this section, three typical HEA systems are chosen to study the validity of current design rules of HEAs

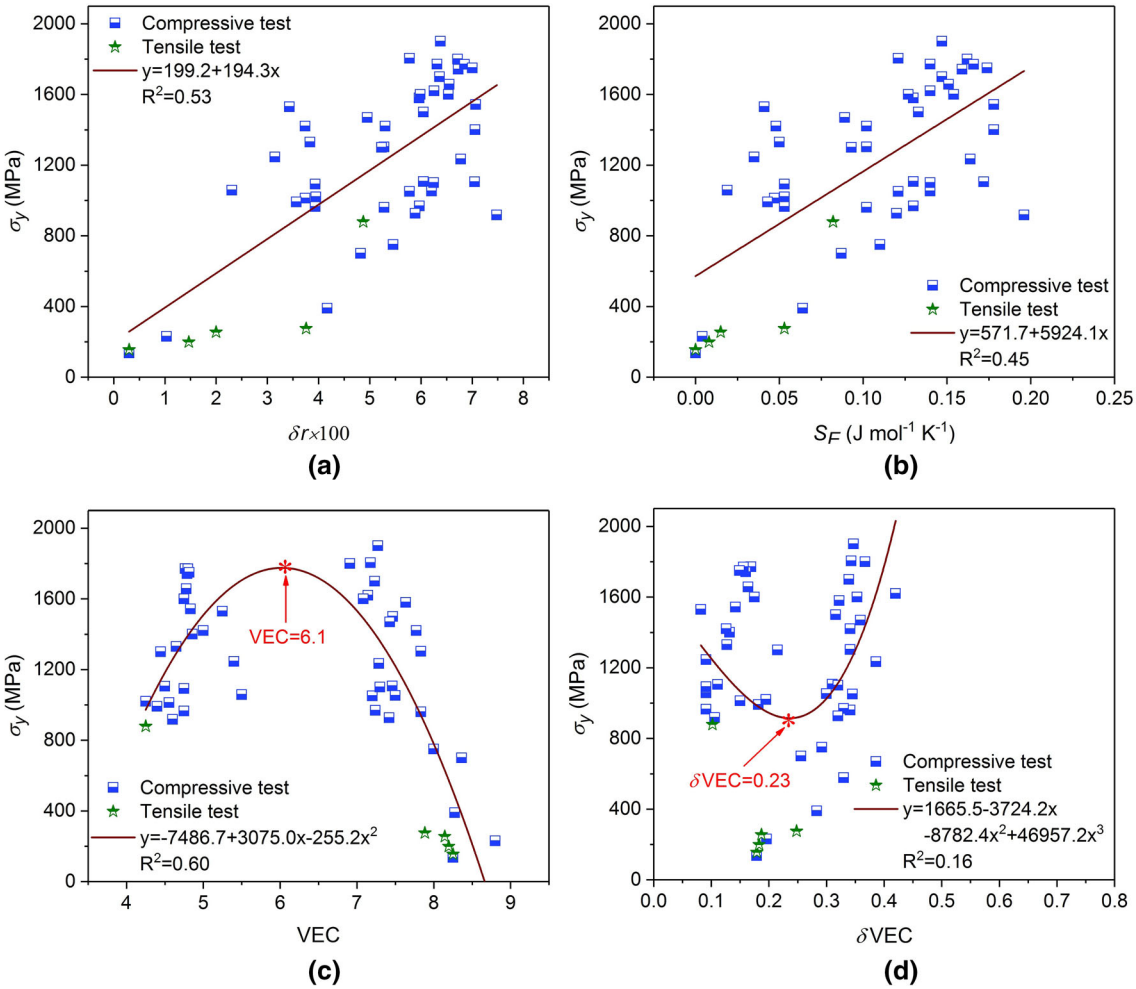

Fig. 7—Yield strength σ_y as a function of (*a*) $\delta r \times 100$, (*b*) S_E, (*c*) VEC, and (*d*) δVEC for HEAs with a single fcc phase, with dual fcc and bcc phases, and with a single bcc phase.

(Table I). Kao *et al.*[63] studied the structures and hardness of the AC, AH, and as-deformed Al_xCoCrFeNi ($0 \le x \le 2$) HEAs. For the AC HEAs, the critical value of x for the transition from HEAs with a single fcc phase (dual fcc and bcc phases) to dual fcc and bcc phases (a single bcc phase) is $x = 0.45$ ($x = 0.88$) at which VEC = 7.72 and δVEC = 0.27 (VEC = 7.30 and δVEC = 0.33). One can see that the decrease of VEC from 7.72 to 7.30 (or the increase of δVEC from 0.27 to 0.33) leads to the structure transition being consistent with the necessary condition for the formation of HEAs with dual fcc and bcc phases, *i.e.*, $6.8 < \text{VEC} < 8.5$ and $0.21 < \delta\text{VEC} < 0.46$. With the increase of x, the value of VEC decreases continuously from VEC = 8.25 for the CoCrFeNi HEA to VEC = 6.50 for the $CoCrFeNiAl_{2.0}$ HEA. Their hardness decreases first and then increases. The maximum (minimum) hardness HV = 509 (110) was obtained by the $CoCrFeNiAl_{2.0}$ ($CoCrFeNiAl_{0.25}$) HEA. Noting that the values of VEC are always smaller than the critical value $\text{VEC}^* \approx 6.13$ at which hardness should be maximum, the increases of HV from the $CoCrFeNiAl_{0.25}$ HEA to the $CoCrFeNiAl_2$ HEA with the decrease of VEC are completely consistent with the current design rules. In addition, δVEC = 0.24 of the $CoCrFeNiAl_{0.25}$ HEA is very near to the critical value $\delta\text{VEC}^* \approx 0.207$ at which hardness should be minimum. Despite the difference in the processing procedures and, thus, hardnesses, the AH and as-deformed Al_xCoCrFeNi ($0 \le x \le 2$) HEAs follow nearly the same rules (Supplementary Tables S-I and S-II).

Tong *et al.*[64] studied the mechanical properties of Al_xCoCrCuFeNi ($x = 0$, 0.5, 1, and 2.5) and found that as x increases, hardness (the compressive yield strength) increases from 133 to 550 (230 to 1620 MPa). Meanwhile, VEC decreases continuously from 8.80 to 7.14 and δVEC increases gradually from 0.20 to 0.42. Noting that the minimum value VEC = 7.14 is smaller than $\text{VEC}^* \approx 6.13$ and δVEC = 0.20 for the CoCrCuFeNi

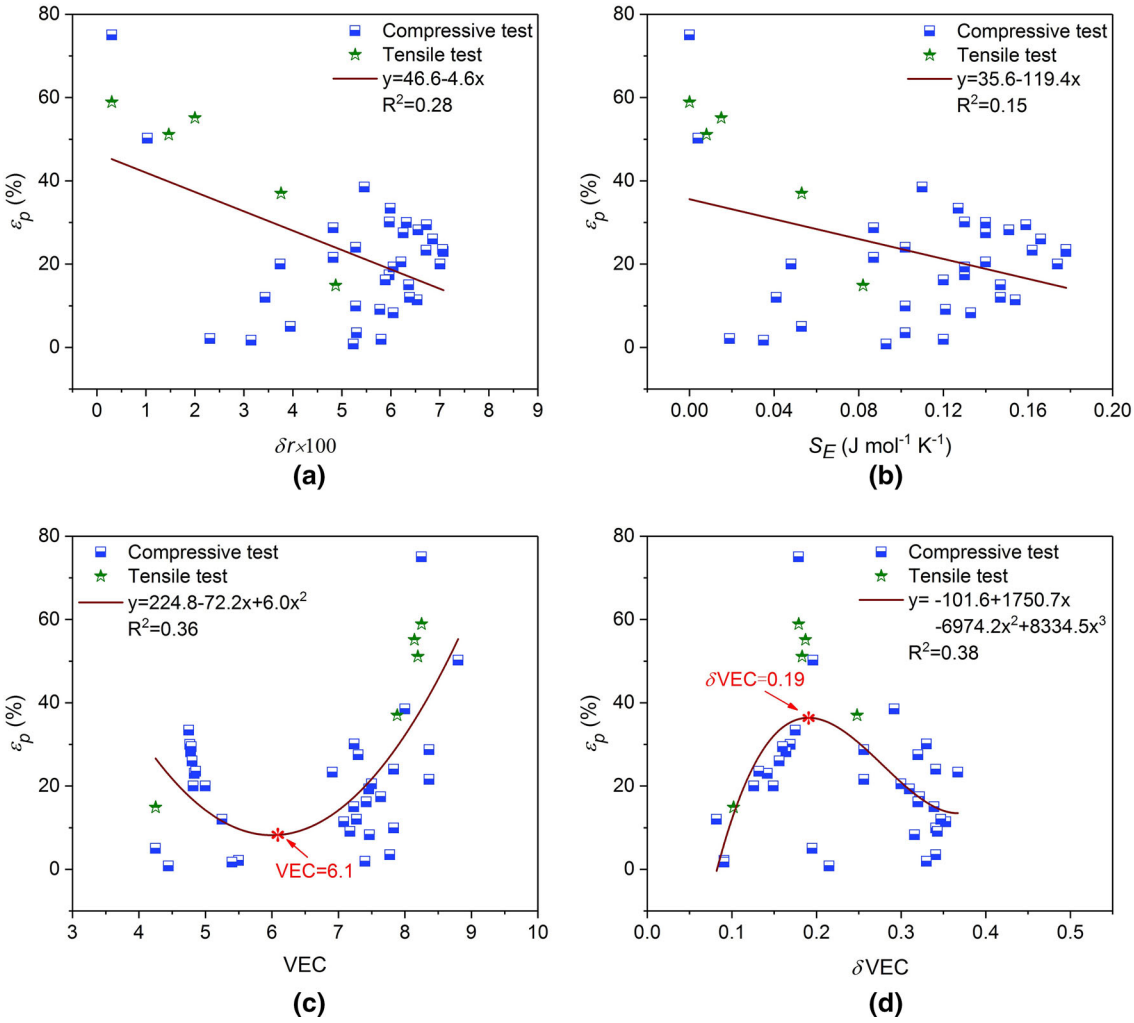

Fig. 8—Plastic strain ε_p as a function of (*a*) $\delta r \times 100$, (*b*) S_E, (*c*) VEC, and (*d*) δVEC for HEAs with a single fcc phase, with dual fcc and bcc phases, and with a single bcc phase.

HEA with the smallest hardness and the yield strength is very near to $\delta VEC^* \approx 0.207$, the current design rules are followed by the $Al_xCoCrCuFeNi$ HEAs. In another work of Wang *et al.*,[65] the $Ti_{0.5}CrFeCoNiAl_xCu_{1-x}$ HEAs were studied. $Ti_{0.5}CoCrFeNiAl_{0.25}Cu_{0.75}$ ($Ti_{0.5}CoCrFeNiAl_{0.75}Cu_{0.25}$) is an HEA with a single fcc (bcc) phase whose yield strength and compressive plastic strain are 750 (1900) MPa and 38.5 pct (12 pct), while the $Ti_{0.5}CoCrFeNiAl_{0.5}Cu_{0.5}$ HEA with dual fcc and bcc phases has a yield strength and a compressive plastic strain of 1580 MPa and 17.4 pct, respectively. The $Ti_{0.5}CoCrFeNiAl_{0.75}Cu_{0.25}$ HEA, whose value of VEC (= 7.27) is nearest to $VEC^* \approx 6.13$, has the highest yield strength. The $Ti_{0.5}CoCrFeNiAl_{0.25}Cu_{0.75}$ HEA, whose value of δVEC (= 0.29) is closest to $\delta VEC^* \approx 0.207$, has the best ductility. All these results indicate that the current design rules are effective for designing HEAs with dual fcc and bcc phases.

V. CONCLUSIONS

The experimental results reported for HEAs with a single fcc phase, with dual fcc and bcc phases, and with a single bcc phase were collected, based on which the design rules for HEAs with dual fcc and bcc phases were studied from structures to mechanical properties. Phase selection between the fcc and bcc phases in HEAs was

Table I. Summary of Standard Deviation of Atomic Radius δr, the Excessive Mixing Entropy Due to the Geometrical Mismatch S_E (J mol^{-1} K^{-1}), the Average VEC and Its Standard Deviation δVEC, the Hardness HV (kgf mm^{-2}), the Yield Strength σ_y (MPa), the Plastic Strain ε_p (Pct) Under Compressive Tests, and the Structure and Processing for the $Al_xCoCrFeNi$ ($0 \le x \le 2$),[63] $Al_xCoCrCuFeNi$ (x = 0, 0.5, 1, and 2.5),[64] and $Ti_{0.5}CrFeCoNiAl_xCu_{1-x}$ (x = 0.25, 0.5, and 0.75)[65] HEAs

HEAs	δr	S_E	VEC	δVEC	HV	σ_y	ε_p	Structure	Processing
CoCrFeNi[63]	0.30	0.00	8.25	0.18	116	—	—	fcc	AC
$CoCrFeNiAl_{0.25}$[63]	3.48	0.05	7.94	0.24	110	—	—	fcc	AC
$CoCrFeNiAl_{0.375}$[63]	4.12	0.06	7.8	0.26	131	—	—	fcc	AC
$CoCrFeNiAl_{0.5}$[63]	4.60	0.08	7.67	0.28	159	—	—	fcc + bcc	AC
$CoCrFeNiAl_{0.75}$[63]	5.30	0.10	7.42	0.32	388	—	—	fcc + bcc	AC
$CoCrFeNiAl_{0.875}$[63]	5.56	0.11	7.31	0.33	538	—	—	bcc	AC
CoCrFeNiAl[63]	5.78	0.12	7.20	0.35	484	—	—	bcc	AC
$CoCrFeNiAl_{1.25}$[63]	6.12	0.14	7.00	0.37	487	—	—	bcc	AC
$CoCrFeNiAl_{1.5}$[63]	6.36	0.15	6.82	0.39	484	—	—	bcc	AC
$CoCrFeNiAl_{2.0}$[63]	6.68	0.16	6.50	0.42	509	—	—	bcc	AC
CoCrCuFeNi[64]	1.03	0.00	8.80	0.20	133	230	—	fcc	AC
$CoCrCuFeNiAl_{0.5}$[64]	3.42	0.04	8.47	0.25	208	390	—	fcc	AC
CoCrCuFeNiAl[64]	5.28	0.1	7.83	0.34	408	960	—	fcc + bcc	AC
$CoCrCuFeNiAl_{2.0}$[64]	6.26	0.14	7.14	0.42	550	1620	—	fcc + bcc	AC
$Ti_{0.5}CoCrFeNiAl_{0.25}Cu_{0.75}$[65]	5.46	0.11	8	0.29	—	750	38.5	fcc	AC
$Ti_{0.5}CoCrFeNiAl_{0.5}Cu_{0.5}$[65]	5.97	0.13	7.64	0.32	—	1580	17.4	fcc + bcc	AC
$Ti_{0.5}CoCrFeNiAl_{0.75}Cu_{0.25}$[65]	6.38	0.15	7.27	0.35	—	1900	12.0	bcc	AC

found to be insensitive to the atomic size difference, the electronegativity difference, the average itinerant electron concentration and its standard deviation, as well as the chemical bond mismatch. The average VEC and its standard deviation are the only parameters that are sensitive to the crystal structure of solid-solution phase. The current work suggests that it is more sensible to design first an HEA with a single fcc (bcc) phase by the necessary condition VEC > 7.7 or $0.17 < \delta\text{VEC} < 0.32$ (VEC < 8.2, δVEC < 0.22 or δVEC > 0.31) and then add other elements with lower (higher) values of VEC. The mechanical properties were found to relate linearly with the atomic size difference. Highest (lowest) hardness, highest (lowest) strength, and lowest (highest) ductility were obtained at nearly the same critical value VEC$^* \approx 6.13$ (δVEC$^* \approx 0.207$), which corresponds to the HEA with a single bcc (fcc) phase. Therefore, a modulation between strength and ductility can be achieved by the HEAs with dual fcc and bcc phases.[66] The validity of the current design rules was tested by application to the $Al_xCoCrFeNi$ ($0 \le x \le 2$), $Al_xCoCrCuFeNi$ (x = 0, 0.5, 1, and 2.5), and $Ti_{0.5}CrFeCoNiAl_xCu_{1-x}$ (x = 0.25, 0.5, and 0.75) HEAs.

ACKNOWLEDGMENTS

This work was done under the Huo Yingdong Young Teacher Fund (Grant No. 151048), the Science Fund for Distinguished Young Scholars from Shaanxi province (Grant No. 2018-JC007), and the Fundamental Research Funds for the Central Universities. The authors appreciate Dr. Vipul Bhardwaj for reading and polishing the manuscript.

ELECTRONIC SUPPLEMENTARY MATERIAL

The online version of this article (https://doi.org/10.1007/s11661-019-05131-1) contains supplementary material, which is available to authorized users.

REFERENCES

1. B. Cantor, I.T.H. Chang, P. Knight, and A.J.B. Vincent: *Mater. Sci. Eng. A*, 2004, vols. 375–377, pp. 213–18.
2. J.W. Yeh, S.K. Chen, S.J. Lin, J.Y. Gan, T.S. Chin, T.T. Shun, C.H. Tsau, and S.Y. Chang: *Adv. Eng. Mater.*, 2004, vol. 6, pp. 299–303.
3. M.H. Tsai and J.W. Yeh: *Mater. Res. Lett.*, 2014, vol. 2, pp. 107–23.
4. B. Gludovatz, A. Hohenwarter, D. Catoor, E.H. Chang, E.P. George, and R.O. Ritchie: *Science*, 2014, vol. 345, pp. 1153–58.
5. Z.M. Li, K.G. Pradeep, Y. Deng, D. Raabe, and C.C. Tasan: *Nature*, 2016, vol. 534, pp. 227–30.
6. Y. Zou, H. Ma, and R. Spolenak: *Nat. Commun.*, 2015, vol. 6, p. 7748.
7. M.H. Chuang, M.H. Tsai, W.R. Wang, S.J. Lin, and J.W. Yeh: *Acta Mater.*, 2011, vol. 59, pp. 6308–17.
8. D.B. Miracle and O.N. Senkov: *Acta Mater.*, 2017, vol. 122, pp. 448–511.
9. A. Abu-Odeh, E. Galvan, T. Kirk, H. Mao, Q. Chen, P. Mason, R. Malak, and R. Arróyave: *Acta Mater.*, 2018, vol. 152, pp. 41–57.
10. A. Tazuddin, N.P. Gurao, and K. Biswas: *J. Alloys Compd.*, 2017, vol. 697, pp. 434–42.
11. Y. Zhang, T.T. Zuo, Z. Tang, M.C. Gao, K.A. Dahmen, P.K. Liaw, and Z.P. Lü: *Progr. Mater. Sci.*, 2014, vol. 61, pp. 1–93.
12. E.J. Pickering and N.G. Jones: *Int. Mater. Rev.*, 2016, vol. 61, pp. 183–202.
13. M.C. Gao, C. Zhang, P. Gao, F. Zhang, L.Z. Ouyang, M. Widom, and J.A. Hawk: *Curr. Opin: Solid State Mater. Sci.*, 2017, vol. 21, pp. 238–51.
14. Y. Zhang, Y.J. Zhou, J.P. Lin, G.L. Chen, and P.K. Liaw: *Adv. Eng. Mater.*, 2018, vol. 10, pp. 534–38.
15. X. Yang and Y. Zhang: *Mater. Chem. Phys.*, 2012, vol. 132, pp. 233–38.

16. A. Takeuchi, K. Amiya, T. Wada, K. Yubuta, W. Zhang, and A. Makino: *Mater. Trans.*, 2014, vol. 55, pp. 165–70.
17. S. Guo and C.T. Liu: *Prog. Nat. Sci. Mater. Int.*, 2011, vol. 21, pp. 433–46.
18. S. Guo, C. Ng, J. Lu, and C.T. Liu: *J. Appl. Phys.*, 2011, vol. 109, p. 103505.
19. S. Sheikh, S. Shafeie, Q. Hu, J. Ahlström, C. Persson, J. Vesel, J. Zýka, U. Klement, and S. Guo: *J. Appl. Phys*, 2016, vol. 120, p. 164902.
20. M.H. Tsai, K.Y. Tsai, C.W. Tsai, C. Lee, C.C. Juan, and J.W. Yeh: *Mater. Res. Lett.*, 2013, vol. 1, pp. 207–12.
21. M.H. Tsai, K.C. Chang, J.H. Li, R.C. Tsai, and A.H. Cheng: *Mater. Res. Lett.*, 2016, vol. 4, pp. 90–95.
22. F.Y. Tian, L.K. Varga, N.X. Chen, J. Shen, and L. Vitos: *Intermetallics*, 2015, vol. 58, pp. 1–6.
23. X. Yang and Y. Zhang: *Mater. Chem. Phys.*, 2012, vol. 132, pp. 233–38.
24. M.G. Poletti and L. Battezzati: *Acta Mater.*, 2014, vol. 75, pp. 97–306.
25. A.K. Singh and A. Subramaniam: *J. Alloys Compd.*, 2014, vol. 587, pp. 113–19.
26. Q.W. Xing and Y. Zhang: *Chin. Phys. B*, 2017, vol. 26, p. 018104.
27. Z.J. Wang, W.F. Qiu, Y. Yang, and C.T. Liu: *Intermetallics*, 2015, vol. 64, pp. 63–69.
28. Z.J. Wang, Y.H. Huang, Y. Yang, J.C. Wang, and C.T. Liu: *Scripta Mater.*, 2015, vol. 94, pp. 28–31.
29. Y.F. Ye, C.T. Liu, and Y. Yang: *Acta Mater.*, 2015, vol. 94, pp. 152–61.
30. A.K. Singh, N. Kumar, A. Dwivedi, and A. Subramaniam: *Intermetallics*, 2014, vol. 53, pp. 112–19.
31. A. Takeuchi, K. Amiya, T. Wada, K. Yubuta, W. Zhang, and A. Makino: *Entropy*, 2013, vol. 15, pp. 3810–21.
32. Y.F. Ye, Q. Wang, J. Lu, C.T. Liu, and Y. Yang: *Scripta Mater.*, 2015, vol. 104, pp. 53–55.
33. A.B. Melnick and V.K. Soolshenko: *J. Alloys Compd.*, 2017, vol. 694, pp. 223–27.
34. O.N. Senkov and D.B. Miracle: *J. Alloys Compd.*, 2016, vol. 658, pp. 603–07.
35. Y.F. Ye, Q. Wang, J. Lu, C.T. Liu, and Y. Yang: *Mater. Today*, 2015, vol. 19, pp. 349–62.
36. Q.F. He, Y.F. Ye, and Y. Yang: *J. Appl. Phys.*, 2016, vol. 120, p. 154902.
37. S. Tripathy, G. Gupta, and S.G. Chowdhury: *Metall. Mater. Trans. A*, 2018, vol. 49A, pp. 7–17.
38. Y.M. Tan, J.S. Li, Z.W. Tang, J. Wang, and H.C. Kou: *J. Alloys Compd.*, 2018, vol. 742, pp. 430–41.
39. Y.M. Tan, J.S. Li, Z.W. Tang, J. Wang, and H.C. Kou: submitted for publication.
40. F. Zhang, C. Zhang, S.L. Chen, J. Zhu, W.S. Cao, and U.R. Kattner: *CALPHAD*, 2014, vol. 5, pp. 1–10.
41. O.N. Senkov, J.D. Miller, D.B. Miracle, and C. Woodward: *Nat. Commun.*, 2015, vol. 6, p. 6529.
42. G. Bracq, M. Laurent-Brocq, L. Perrière, R. Pirès, J.M. Joubert, and I. Guillot: *Acta Mater.*, 2017, vol. 128, pp. 327–36.
43. F. Tian, L. Delczeg, N. Chen, L.K. Varga, J. Shen, and L. Vitos: *Phys. Rev. B*, 2013, vol. 88, p. 085128.
44. P. Singh, A.V. Smirnov, and D.D. Johnson: *Phys. Rev. B*, 2015, vol. 91, p. 224204.
45. D. Ma, B. Grabowski, F. Körmann, J. Neugebauer, and D. Raabe: *Acta Mater.*, 2015, vol. 100, pp. 90–97.
46. C. Jiang and B.P. Uberuaga: *Phys. Rev. Lett.*, 2016, vol. 116, p. 105501.
47. M.C. Troparevsky, J.R. Morris, P.R.C. Kent, A.R. Lupini, and G.M. Stocks: *Phys. Rev. X*, 2015, vol. 5, p. 011041.
48. D.J.M. King, S.C. Middleburgh, A.G. McGregor, and M.B. Cortie: *Acta Mater.*, 2016, vol. 104, pp. 172–79.
49. Y. Wang, M. Yan, Q. Zhu, W.Y. Wang, Y.D. Wu, X.D. Hui, R. Otis, S.L. Shang, Z.K. Liu, and L.Q. Chen: *Acta Mater.*, 2018, vol. 143, pp. 88–101.
50. S. Guo, C. Ng, and C.T. Liu: *J. Alloy Compd.*, 2013, vol. 557, pp. 77–81.
51. Y.P. Lu, Y. Dong, S. Guo, L. Jiang, H.J. Kang, T.M. Wang, B. Wen, Z.J. Wang, J.C. Jie, Z.Q. Cao, H.H. Ruan, and T.J. Li: *Sci. Rep.*, 2014, vol. 4, p. 6200.
52. Y.P. Lu, X.Z. Gao, L. Jiang, Z.N. Chen, T.M. Wang, J.C. Jie, H.J. Kang, Y.B. Zhang, S. Guo, H.H. Ruan, Y.H. Zhao, Z.Q. Cao, and T.J. Li: *Acta Mater.*, 2017, vol. 124, pp. 143–50.
53. Y. Dong, X.X. Gao, Y.P. Lu, T.M. Wang, and T.J. Li: *Mater. Lett.*, 2016, vol. 169, pp. 62–64.
54. J.Y. He, W.H. Liu, H. Wang, Y. Wu, X.J. Liu, T.G. Nieh, and Z.P. Lu: *Acta Mater.*, 2014, vol. 62, pp. 105–13.
55. J.W. Wu, S.J. Lin, J.W. Yeh, S.K. Chen, Y.S. Huang, and H.C. Chen: *Wear*, 2006, vol. 261, pp. 513–19.
56. R.R. Chen, G. Qin, H.T. Zheng, L. Wang, Y.Q. Su, Y.L. Chiu, H.S. Ding, J.J. Guo, and H.Z. Fu: *Acta Mater.*, 2018, vol. 144, pp. 129–37.
57. U. Mizutani: *Hume-Rothery Rules for Structurally Complex Alloy Phases*, CRC Press, Boca Raton, FL, 2010.
58. A. Takeuchi and A. Inoue: *Mater. Trans. JIM*, 2000, vol. 41, pp. 1372–78.
59. A. Takeuchi and A. Inoue: *Mater. Trans.*, 2005, vol. 46, pp. 2817–29.
60. A. Takeuchi and A. Inoue: *Mater. Sci. Eng. A*, 2001, vols. 304–306, pp. 446–51.
61. G.A. Mansoor, N.F. Carnahan, K.E. Starling, and T.W. Leland: *J. Chem. Phys.*, 1971, vol. 54, pp. 1523–25.
62. Y. Zhang, X.H. Yan, W.B. Liao, and K. Zhao: *Entropy*, 2018, vol. 20, p. 624.
63. Y.F. Kao, T.J. Chen, S.K. Chen, and J.W. Yeh: *J. Alloys Compd.*, 2009, vol. 488, pp. 57–64.
64. C.J. Tong, Y.L. Chen, and J.W. Yeh: *Metall. Mater. Trans. A*, 2006, vol. 36A, pp. 1263–71.
65. F.J. Wang, Y. Zhang, and G.L. Chen: *J. Alloys Compd.*, 2009, vol. 478, pp. 321–32.
66. N. Liu, C. Chen, I.T.H. Chang, P. J. Zhou, and X.J. Wang: *Materials,* 2018, vol. 11, pp. 1290, 1–11.